AD-A185 686 PHOTOIONIZATION OF ATOMS AND IONS: APPLICATION OF TIME-DEPENDENT RESPONSE..(U) NAVAL RESEARCH LAB WASHINGTON DC U GUPTA ET AL. 13 OCT 87 NRL-MR-6089 1/1

UNCLASSIFIED MIPR-DGAM-60091 F/G 20/5 NL

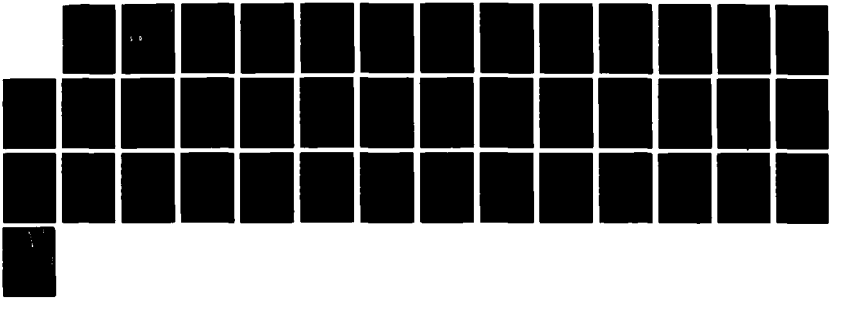

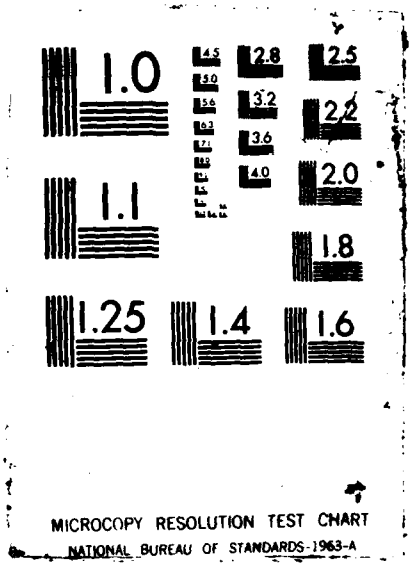
1.0
1.1
1.25
1.4
1.6
1.8
2.0
2.2
2.5
2.8
3.2
3.6
4.0
4.5
5.0
5.6
6.3
7.1
MICROCOPY RESOLUTION TEST CHART
NATIONAL BUREAU OF STANDARDS-1963-A

Naval Research Laboratory

Washington, DC 20375-5000

NRL Memorandum Report 6089

Photoionization of Atoms and Ions: Application of Time-Dependent Response Method Within the Density Functional Theory

U. GUPTA

Berkeley Research Associates
Springfield, VA 22150

J. DAVIS

Plasma Radiation Branch
Plasma Physics Division

M. BLAHA

University of Maryland
College Park, MD

October 13, 1987

A185 686

SECURITY CLASSIFICATION OF THIS PAGE

REPORT DOCUMENTATION PAGE

1a. REPORT SECURITY CLASSIFICATION UNCLASSIFIED	1b. RESTRICTIVE MARKINGS
2a. SECURITY CLASSIFICATION AUTHORITY	3. DISTRIBUTION/AVAILABILITY OF REPORT Approved for public release; distribution unlimited.
2b. DECLASSIFICATION/DOWNGRADING SCHEDULE	
4. PERFORMING ORGANIZATION REPORT NUMBER(S) NRL Memorandum Report 6089	5. MONITORING ORGANIZATION REPORT NUMBER(S)
6a. NAME OF PERFORMING ORGANIZATION Naval Research Laboratory 6b. OFFICE SYMBOL (If applicable) Code 4720	7a. NAME OF MONITORING ORGANIZATION
6c. ADDRESS (City, State, and ZIP Code)	7b. ADDRESS (City, State, and ZIP Code)
8a. NAME OF FUNDING/SPONSORING ORGANIZATION Strategic Defense Initiative Organization 8b. OFFICE SYMBOL (If applicable) IST	9. PROCUREMENT INSTRUMENT IDENTIFICATION NUMBER
8c. ADDRESS (City, State, and ZIP Code) Washington, DC 20301-7100	10. SOURCE OF FUNDING NUMBERS PROGRAM ELEMENT NO. 63220C; PROJECT NO.; TASK NO.; WORK UNIT ACCESSION NO. 017L7

11. TITLE (Include Security Classification)
Photoionization of Atoms and Ions: Application of Time-Dependent Response Method Within the Density Functional Theory

12. PERSONAL AUTHOR(S)
Gupta, U., Davis, J. and Blaha, M.

13a. TYPE OF REPORT	13b. TIME COVERED	14. DATE OF REPORT (Year, Month, Day)	15. PAGE COUNT
Interim	FROM _____ TO _____	1987 October 13	41

16. SUPPLEMENTARY NOTATION
This work was supported by the Strategic Defense Initiative Organization under Job Order Title, Ultra Short Wavelength Laser Research, MIPR Number DGAM60091.

17. COSATI CODES		
FIELD	GROUP	SUB-GROUP

18. SUBJECT TERMS (Continue on reverse if necessary and identify by block number)
Photoionization; Density functional; Atoms; Time dependent

19. ABSTRACT (Continue on reverse if necessary and identify by block number)

The photoionization cross-section of several atoms (Ar, Xe, Rn, Cs) and ions (Ne-like Ar, H-like and Li-like C) of experimental interest are calculated using the time-dependent response scheme within the framework of local density functional method (DFM). The cross-sections for rare gas atoms calculated using this method agree very well with the experimental data; whereas conventional independent particle model calculations do not. The polarization effect of the atom brought about by the incident time-varying radiation field is shown to be important in describing observed results. Unlike the independent particle model, this effect is treated adequately in the DFM.

To study the effect plasma density and temperature on the photoionization cross-section, calculations were also done for the ions mentioned above at various densities and temperatures. For computational simplicity, a simplified model of self-consistent finite temperature DFM was used in which the long range part of the ionic potential was taken as the Debye-screened potential. These calculations were compared with the isolated ion calculations (without any plasma effect). With increasing plasma density, significant shifts of the ionization threshold as well as substantial modifications of photoionization cross-section are obtained. This points out the need for incorporating the effect of surrounding plasma in realistic modeling of atomic properties for dense plasmas.

20. DISTRIBUTION/AVAILABILITY OF ABSTRACT ☒ UNCLASSIFIED/UNLIMITED ☐ SAME AS RPT ☐ DTIC USERS	21. ABSTRACT SECURITY CLASSIFICATION
22a. NAME OF RESPONSIBLE INDIVIDUAL Dr. Jack Davis	22b TELEPHONE (Include Area Code) (200) 767-3278 22c. OFFICE SYMBOL Code 4720

DD FORM 1473, 84 MAR 83 APR edition may be used until exhausted. All other editions are obsolete

SECURITY CLASSIFICATION OF THIS PAGE

CONTENTS

Photoionization of Atoms and Ions: Application of Time-Dependent Response Method Within the Density Functional Theory

I. INTRODUCTION

Accurate calculation of photoionization and photoexcitation cross-sections of atoms and ions are useful in a variety of investigations in plasma physics and atomic physics. It is particularly useful in the context of flashlamp photopumping schemes for x-ray lasers. Most of the existing calculations of photoionization cross-sections were done using the single electron or the independent particle model (IPA). In this model, the energy-levels, and wavefunctions of the atom or ion are first calculated using the Hartree-Fock (HF) method. The interaction of the incident electromagnetic radiation with the atom (or ion) is treated via the first order perturbation theory.

Comparison of experimental data with the IPA calculations shows that for some simple systems such as a neutral few electron atom (Lithium, for example), there is qualitative and sometimes quantitative agreement. However, for many electron atoms (Xenon, for example) and ions with a large number of bound electrons, substantial discrepencies are found between experimental and IPA-data.[1]

In our work, we used the time-dependent linear response approximation within the framework of the relativistic density functional method (DFM)[2,3,4] to treat the problem of photoionization. This method incorporates certain advantages over the HF-method. The HF-method is non-local and computationally very elaborate, whereas in the density functional method, one deals with a set of local equations only. This leads to computational simplicity. On the other hand, it is well known from extensive application of the density functional method, that fairly accurate atomic energy levels, wavefunctions etc. are obtained. The computational simplicity is even more apparent in the case of relativistic DFM versus relativistic HF-methods. In the DFM, correlation effects of

Manuscript approved July 29, 1987.

the bound electrons in the atom are accounted for in a simple way via the correlation potential. The Hartree-Fock method, on the other hand, does not take into account electron correlation, although it accounts for non-local exchange effects appropriately.

The independent particle method does not take into account the polarization effect of the atom brought about by the incident time-varying radiation field. In the linear response method within the density functional method, this is treated adequately - as will be seen from comparison with the experimental data. In most experimental situations, the incident radiation (from synchrotron sources or lasers) have field strengths small compared to the atomic field strengths. For those experimental conditions, the present model based on linear response is adequate and useful.

Calculations of photoionization and photoexcitation cross-sections and rates have a number of applications. For the photopumping scheme for x-ray lasers, these processes play a crucial role in contributing to a population inversion of excited ionic levels. As another example, computation of opacities of plasmas for diagnostic and target response effects require these data as input. In order to model the radiation spectra from hot plasmas (via detailed configuration rate equation technique, for example), the photoionization and photoexcitation data are required in addition to other bound-bound, bound-free and free-free processes. Acccurate calculations are also necessary for interpreting experimentally available data on cross-sections. In view of these different applications, there is a need for realistic modeling of these processes in order to generate accurate data over a wide range of photon energy for a variety of atoms and ions. The present model provides such a tool and its usefulness will be discussed in subsequent sections.

The above discussion deals with the calculation of photoionization of isolated atoms or ions - that is, without the effect of the plasma environment. These effects are negligible for very low density plasmas. In many experimental situations, however, the plasma density can be quite high (for example, in laser produced plasmas). In those cases, additional effects due to screening shifts of energy levels and modification of wavefunctions and potentials for the ion embedded in high density plasmas have to be considered. In the later part of this report, we will present some results of photoionization cross-section of ions in a dense plasma medium and examine the modification of cross-sections due to the plasma environment.

II. THE METHOD OF CALCULATION

The first part of the calculation is to generate the energy-level spectrum and the wavefunctions of the particular atom or ion of specific configuration. This is done by using the local density functional method. In order to treat many-electron atoms (with high Z) appropriately, relativistic DFM equations were used. In this method, the following set of equation were solved self-consistently:

$$\left[c\,\vec{\alpha}\cdot\vec{p} + c^2\beta + u(\vec{r})\right]\psi_i(\vec{r}) = E_i\,\psi_i(\vec{r}) \qquad (1)$$

$$u(r) = -\frac{Z}{r} + \int \frac{\rho(\vec{r}')\,d\vec{r}'}{|\vec{r}-\vec{r}'|} + \frac{\partial}{\partial\rho(\vec{r})}\left[\rho(\vec{r})\,\varepsilon_{xc}(\rho(\vec{r}))\right] \qquad (2)$$

$$\text{and } \rho(\vec{r}) = \sum_i f_i\,|\psi_i(\vec{r})|^2 \qquad (3)$$

In the above, $\rho(\vec{r})$ is the electronic charge density of the atom, $\vec{\alpha}$'s are the Dirac matrices, f_i's are the integral occupation factors corresponding to the number of electrons in each state $\psi_i(r)$ with corresponding energy eigenvalue E_i. The atomic potential u(r)

contains, in addition to the nuclear and the electrostatic Hartree term, a contribution arising from the electron exchange and correlation effects. Let us note that the use of integer occupation factors f_i's for the given configuration distinguishes this model from the "average atom model" where the occupation factors are taken to be those given by the statistical Fermi distribution function.

The orbital functions are four-component spinors. They are split into major and minor components:

$$\psi(\vec{r}) = \begin{pmatrix} \psi^1(\vec{r}) \\ \psi^2(\vec{r}) \end{pmatrix} = \begin{pmatrix} (A(r)/r)\ i^l\ \Omega_{jlm}(\hat{r}) \\ (B(r)/r)\ i^l\ \Omega_{jl'm}(\hat{r}) \end{pmatrix} \tag{4}$$

where A and B are major and minor components of the radial functions and Ω_{jlm} and $\Omega_{jl'm}$ are two-component Pauli spinors with the indicated numbers. The various quantum numbers are related by

$$l' = l + S,\ j' = l + 1/2,\ S = l' - 1/2\ S,\ K = -S\ (j + 1/2);\ S = \pm 1 \tag{5}$$

The differential equations for A and B (in matrix form) are:

$$\frac{d}{dr}\begin{pmatrix} A \\ B \end{pmatrix} = \begin{pmatrix} -K/r & (u - E - c^2)/cs \\ -(u - E + c^2)/cs & K/r \end{pmatrix} \begin{pmatrix} A \\ B \end{pmatrix} \tag{6}$$

In Eq. (2), ε_{xc} is the exchange-correlation energy of the electrons. In actual calculation, Gunnarsson-Lundquist (G-L) form[3] for exchange-correlation energy and potential was used. It is well known that reliable atomic data is obtained from the use of G-L exchange-correlation. Equations (1) - (6) are solved numerically to self-consistency to obtain the wavefunctions ψ_i's, the binding energies of each orbital E_i, the atomic charge density $\rho(\vec{r})$ and the self-consistent potential $u(\vec{r})$.

Now consider the effect of an incident time-varying radiation field $E(t) = E_o e^{i\omega t}$ on the atom. It induces a time-dependent atomic density deviation, $\delta\rho(\vec{r},t)$, causing a time-dependent polarization effect. For the linear response method used here, it is convenient to work with the Fourier transform:

$$\delta\rho(\vec{r},\ t) = \frac{1}{2\pi} \int_{-\infty}^{\infty} \delta\rho(\vec{r},\omega) e^{-i\omega t}\, d\omega \tag{7}$$

The net induced density due to the external plus the induced potential is

$$\delta\rho_{ind}\ (\vec{r},\omega) = \int \chi(\vec{r},\vec{r}',\omega)\ \left[V_{ext}(\vec{r},\omega) + V_{ind}\ (\vec{r},\omega)\right] d\vec{r}', \tag{8}$$

where the induced potential is given by

$$V_{ind}(\vec{r},\omega) = \int \frac{\delta\rho(\vec{r}',\ \omega)}{\vec{r} - \vec{r}'}\ d\vec{r}' + \frac{\partial V_{xc}(\rho(\vec{r}))}{\partial\rho(\vec{r})}\ \delta\rho(\vec{r},\omega) \tag{9}$$

The response function is given by

$$\chi\ (\vec{r},\vec{r}',\omega) = \sum_i f_i \psi_i^*(\vec{r})\ \psi_i(\vec{r}')\ G\ (\vec{r},\vec{r}',\ E_i + \omega) \tag{10}$$

$$+ \sum_i f_i\ \psi_i(\vec{r})\ \psi_i^*\ (\vec{r}')\ G^*\ (\vec{r},\vec{r}',\ E_i - \omega)$$

and thus involves the wavefunctions and energy levels of the atom. The Green's functions are solutions of the inhomogeneous Dirac equation

$$(c\vec{\alpha}\ .\ \vec{p} + c^2\beta + u\ (r) - E)\ G\ (\vec{r},\vec{r}',\ E) = -\ \delta(\vec{r} - \vec{r}') \tag{11}$$

In actual calculation, angular decomposition of the Green's function in terms of spherical harmonics is done (Appendix I) and the radial part is treated separately.

The frequency dependent polarizability $\alpha(\omega)$ is the ratio of the induced dipole moment to the external field:

$$\alpha(\omega) = -\frac{e}{E_o}\int Z\ \delta\rho\ (\vec{r},\omega)\ d\vec{r} \tag{12}$$

Note that $\alpha(\omega)$ like $\delta\rho(\vec{r},\omega)$ is complex. The induced density deviation (and also the corresponding induced potential) can have a phase difference with respect to that of the applied external field. Once $\alpha(\omega)$ is determined, the photoabsorption cross-section $\sigma(\omega)$ of the atom is obtained from:

$$\sigma(\omega) = \frac{4\pi\omega}{c}\ \text{Im}\ \alpha\ (\omega). \tag{13}$$

III. PARTIAL CROSS-SECTION

In order to see the connection with the IPA-model, consider the partial cross-section due to photoionization from a specific bound state $\psi_i(\vec{r})$ to a final continuum state $\psi_f\ (\vec{r})$.

The initial atomic state is represented as

$$\psi_i(\vec{r}) = \frac{U_{nl}(r)}{r}\ Y_L\ (\hat{r}) \tag{14}$$

and the final continuum state with wavevector $\vec{K}$ and energy ε as

$$\psi_f(\vec{r}) = 4\pi \sum_{L'} A_{l'} i^{l'}\ \frac{P_{\varepsilon l'}(r)}{r}\ Y^*_{L'}\ (\hat{K})\ Y_{L'}(\hat{r}) \tag{15}$$

The complex coefficients $A_{l'}$s are found by requiring $\psi_f(r)$ to behave asymptotically as an incident plane wave plus a spherical wave. Then the partial cross-section σ_{nl} is shown to be

$$\sigma_{nl}(\omega) = 2\ (2l+1)\ \alpha\hbar\ \omega\ \sqrt{\varepsilon}\ a_B^2$$

$$\times \sum_{L'} |A_{l'}|^2\ |\langle l\ 100|\ l'0\rangle|^2\ \left|\int P_{\varepsilon l'}(r)\ V^{SCF}(r,\omega)\ U_{nl}(r)\ dr\right|^2 \tag{16}$$

where $\langle l\ 100|\ l'0\rangle$ is a Clebsch-Gordon coefficient.

In (16), $V^{SCF}(r,\omega)$ is a frequency dependent complex self-consistent potential. Note that, if $V^{SCF}(r,\omega)$ is replaced by the usual dipole moment operator, one obtains the conventional or independent particle approximation (IPA) result. In actual calculations, both bound and continuum wavefunctions are generated numerically using the Numerov method for integrating the Dirac equation. Let us also note that the real and imaginary parts of the self-consistent field contributes to the partial cross-section without interference. Computations were performed for both the conventional independent particle model and the time-dependent linear response to density functional method for comparison purposes.

IV. RESULTS

In Fig. 1, results of computed photoionization cross-section for neutral xenon is plotted as a function of photon energy near the 4d-threshold. The drastic difference between the results obtained from the time-dependent response method (curve A) and from conventional IPA-model (curve B) is clear. The IPA-model does not reproduce the experimental values[5] at all whereas the present time-dependent model agrees very well with the experimental data over this entire range of photon energy from 5 to 10 Ryd., including the peak at about 7 Ryd. In that energy range, the IPA cross-section shows a rapid decrease - in contrast to the experimental data.

The primary physical reason for this difference in the two models arise from the polarization effect of the atom subjected to the incident radiation. In the case of xenon, all of the 54 bound

electrons forming the atom participate in the polarization process (the outer ones contributing most). The external field is screened in the energy range 5-6 Ryd. (and again in the range 8.5 - 9.5 Ryd.), and is antiscreened in the intermediate 6-8 Ryd. range. The antiscreening effect produces a stronger effective field for the 4d-electron to photoionize, thereby enhancing the cross-sections somewhat in the intermediate energy range as seen in Fig. 1.

The 3s-partial cross-section for Argon is shown in Fig. 2. The experimental data[7] in the range of 30 - 65 eV are depicted by circles with the error bars. The conventional IPA-calculation (curve A) again does not show the experimentally seen variation at all. The present time dependent response method reproduces the observed variation including the experimental Cooper minimum at about 43 eV and is in good agreement with the measured cross-sections. The occurrence of the Cooper minimum is known[1] to be due to the vanishing of the matrix element between bound and continuum states at that photon energy. In the present time-dependent polarization model, the physical reason for the minimum is that the induced potential almost exactly cancels out the external field, reducing the effective field to almost zero.

The total cross-section for Argon atom as a function of the photon energy is plotted in Fig. 3, and compared with experimental data[8]. Comparison is also made of results obtained from Hartree-Fock (HF) length and velocity approximations by Kennedy and Manson[6]. We note that the time-dependent response model again best reproduces the experimental data. The HF-velocity approximation gives, for example, a cross-section twice as large at 40 eV whereas the HF-length result is six times larger than the experimental data at the same photon energy.

Good agreement with available experimental data for Ar, Ne, Kr and Xe suggests that reliable cross-sections can also be generated for higher-Z rare gas atoms such as Radon utilizing the time-dependent response model. For Radon (Z=86), relativistic effects are significant. The Dirac equation approach in our model is therefore suitable. We performed self-consistent calculation for Radon and the computed total cross-section is plotted in Fig. 4 for the photon energy range 7-28 eV. The large difference between the results obtained from IPA-model and the present time-dependent response model is clearly seen from the graph. The large peaks due to the ionization from $6P_{1/2} \rightarrow d_{3/2}$ in the IPA-model are masked significantly due to polarization effect incorporated in the time-dependent response model. No experimental data is available for the case of Radon. However, in view of the good agreement between experimental data and the results of time-dependent response model, it is expected that future experimental measurements for Radon in this photon energy range will be in close agreement with these calculated cross-sections.

The 6s partial cross-section for Cesium as a function of photon energy in the range of 4-8 eV is plotted in Fig. 5. In this particular case, there are significant differences in the two sets of experimental data[9,10] of the two groups, presumably due to uncertainties in vapor pressure measurement. Calculated value of partial cross-sections from the time-dpendent model is in fair agreement with one set of observed data (Fig. 5). The effect of spin-orbit interaction is known to be significant for the 6s partial cross-section of Cesium. A more detailed theory should incorporate this effect. As seen from Fig. 5, the IPA-model shows a monotonic decrease of cross-section in this energy range in complete disagreement with the experimental data.

Ions of specific configurations such as Neon-like Argon are of interest for scaling to higher Z neonlike systems for x-ray laser research. No experimental data is available for these ions and thus the data have to be provided by theoretical calculations. The fact that the time-dependent response method is successful for generating accurate data for rare gas atoms suggests that reliable cross-sections can be generated for Ne-like Ar and other ions of interest. Computed results for Ne-like Argon are presented in Fig. 6 and compared with conventional IPA-calculations. The differences are smaller in this case, as expected, because the number of bound electrons for these ions is only ten. For these highly charged ions, these electrons are very tightly bound and thus do not participate as effectively in the polarization process.

The results presented above are for single atoms or ions without the effect of the plasma environment - as appropriate for very low density plasmas. For high density plasmas, however, effects due to screening shifts of energy levels, modification of wavefunctions of bound (particularly the upper levels) and continuum wavefunctions as well as potentials of the ion embedded in the plasma have to be considered.

For proper treatment these effects, the self-consistent density functional method (DFM) at finite temperatures[11] should be used. The application of this method requires iterative numerical solution of Schrodinger equation involving the complete set of bound and continuum wavefunctions for the multielectron ion and construction of effective potential inclusive of plasma screening and electronic exchange correlation effect in each iteration. For our present purpose, we adopted the following simplified approach for computational simplicity. For a given plasma density and temperature, we represent

the long range part of the effective potential in the Debye-screened form. The inner part of the effective potential was constructed by numerical itegration of the Hartree term with the electron density distribution calculated using the bound state wavefunctions.

The results of our calculation for H-like and Li-like carbon ions are shown in figures 7-11. From fig. 7, we see, by comparing with isolated atom cross-sections, that the threshold for photoionization from 1s-level of H-like C shifts substantially (from 18 eV to about 15.2 eV) for Debye length λ_D = 2 a.u. This is significant in the context of calculation of photoionization rates, which is calculated by integrating the cross-section weighted by the electron distribution function (usually the Maxwell-Boltzmann distribution) over the entire energy range. The calculated rates in the two cases would therefore be very different - as seen from fig. 7.

In fig. 8, the corresponding results of partial photoionization cross-section for H-like C is plotted. Fig. 9 shows the 3d-partial cross-sections of the same ion at two different plasma conditions (λ_D = 5 and 2 a.u.) and compared with the isolated atom cross-section (curve A). The increasing shift of the ionization threshold with decreasing λ_D (i.e. with increasing density) clear from the figure 9.

We performed similar calculation for Li-like carbon as well (fig. 10-11). Since there are three bound electrons for these ions, iterative calculations mentioned before was performed for the bound states and the continuum wavefunction was computed with 1-electron removed (by ionization) from the given state 2s or 3s. Comparison

with isolated ion results shows substantial modification of photoionization cross-section at these densities and temperatures and significant shifts of ionization threshold due to effect of the surrounding plasma.

V. CONCLUSIONS

It is demonstrated that the time-dependent linear response method within the framework of local relativistic density functional theory can provide reliable atomic data for various atoms and ions of experimental interest. This model is particularly useful in those situations where conventional independent particle models fail to provide accurate data. The mechanism of time-dependent polarization of the atom is seen to be important in describing the observed results. As a practical point, the computer code based on the time-dependent model is fast and efficient, capable of generating a large number of data in a short time (for example, cross-sections for 10 photon energies for a medium-Z atom takes about 3 minutes of c.p.u. time on a Cray-XMP computer). The present method is capable of treating large complex atoms with high-Z for which relativistic effects are important. Let us point out that if the applied radiation field strength is very high, so that it is comparable or larger than the atomic field strength, new extensions or developments of the present model is necessary to treat those conditions. Full numerical solution of time-dependent density functional method (beyond the linear response approximation) would be one suitable to use in those cases. Work in this new direction is planned for the future.

With reference to the calculations for the different plasma conditions, let us point out that the Debye-screened form for the long range part of the potential may not be adequate for the high-density plasmas. For more realistic calculation, it is necessary to use fully self-consistent finite temperature density functional method for those plasma conditions. Also, the effect of exchange and correlation for plasma electrons become important at high densities. The present approximate scheme is used at present for computational simplicity. However, the results shown here clearly indicate that with increasing plasma density, the photoionization cross-section and rates of the ions forming the plasma can be substantially modified. Accurate modeling of atomic properties for dense plasmas, therefore, requires that the effect of the surrounding plasma should be properly included in the calculation.

Acknowledgment:

This work is supported in part by the AFOSR, ONR and SDIO/IST. The authors wish to thank J. Pender of Berkeley Research Assoc. for his help in plotting the diagrams and Dr. K. Whitney of NRL for useful discussions.

Appendix I

The Green's function G in eq. (11) has 16 components, which are represented in matrix form

$$G(\vec{r}, \vec{r}', E) = \begin{pmatrix} G^{11}(\vec{r},\vec{r}'| E) & G^{12}(\vec{r},\vec{r}'| E) \\ G^{21}(\vec{r},\vec{r}'| E) & G^{22}(\vec{r},\vec{r}'| E) \end{pmatrix}$$

The angular decompositon of various terms are

$$\begin{aligned} G^{11}(\vec{r},\vec{r}'|E) &= \sum_{jlm} \Omega_{jlm}(\hat{r})\, G^{11}_{jl}(r,r'|E)\, \Omega^{*}_{jlm}(\hat{r}') \\ G^{12}(\vec{r},\vec{r}'|E) &= \sum_{jlm} i^{l-l'}\, \Omega_{jlm}(\hat{r})\, G^{12}_{jl}(r,r,',|E)\, \Omega^{*}_{jlm}(\hat{r}') \\ G^{21}(\vec{r},\vec{r}'|E) &= \sum_{jlm} i^{l'-l}\, \Omega_{jl'm}(\hat{r})\, G^{21}_{jl}(r,r'|E)\, \Omega^{*}_{jlm}(\hat{r}') \\ G^{22}(\vec{r},\vec{r}'|E) &= \sum_{jlm} \Omega_{jl'm}(\hat{r})\, G^{22}_{jl*}(r,r'|E)\, \Omega^{*}_{jl'm}(\hat{r}') \end{aligned} \qquad \text{(I-2)}$$

The radial part $G^{\alpha\beta}(r,r' E)$ are solutions of the radial inhomogeneous Dirac equation

$$G^{\alpha\beta}_{jl}(r,r'|E) = \begin{cases} \upsilon^{\alpha}_{jl}(r)\ \bar{\upsilon}^{\beta}_{jl}(r') / (rr'W_{jl}) & r < r' \\ \upsilon^{\alpha}_{jl}(r)\ \upsilon^{\beta}_{jl}(r') / (rr'W_{jl}) & r > r' \end{cases} \qquad \text{(I-3)}$$

W_{jl} is the Wronskian

$$W_{jl} = -cS_{jl}\left[\upsilon^{2}_{jl}(r)\ \bar{\upsilon}^{1}_{jl}(r) - \bar{\upsilon}^{2}_{jl}(r)\ \upsilon^{1}_{jl}(r)\right] = \text{const.}$$

$\bar{\upsilon}^{1}_{jl}(r)$ and $\bar{\upsilon}^{2}_{jl}(r)$ are major and minor component radial functions that are real and regular at r = o. $\bar{\upsilon}^{1}{}_{jl}(r)$ and $\bar{\upsilon}^{2}{}_{jl}(r)$ major and minor component

radial functions which (for $E > c^2$) are complex and obey outgoing wave boundary conditions at $r = \infty$. The phase for $\bar{v}^1_{jl}$ and $\bar{v}^2_{jl}$ is chosen so that W_{jl} is real. When $E < c^2$, $\bar{v}^1_{jl}(r)$ and $\bar{v}^2_{jl}(r)$ are real and decay exponentially at large radii.

With the above representations, the polarizability $\chi(r,r'\ \omega)$ is given by

$$\chi_j\ (r,r'\ \omega) = \Sigma\ f_i\ (2j_2+1)\ (2l_1+1)\ (2l_2+1)\ x$$

$$\left[\begin{pmatrix} l_1 & l_2 & I \\ o & o & o \end{pmatrix} \begin{pmatrix} I & l_1 & l_2 \\ 1/2 & j_2 & j_1 \end{pmatrix} \right]^2 x\ \frac{1}{W_{j_2 l_2}(E_i \pm \omega)} \left[A_i(r) v^1_{j_2 l_2}(r|\ \varepsilon_i \pm \omega) \right.$$

$$\left. \pm\ i^{S_1 - S_2}\ B_i(r)\ v^2_{j_2 l_2}(r\ \ \varepsilon_i \pm \omega) \right] x \left[A_i(r')\ \bar{v}\ {}^1_{j_2 l_2}(r'|\ \varepsilon_i \pm \omega) \right.$$

$$\left. \pm\ i^{S_2 - S_1}\ B_i(r')\ \bar{v}\ {}^2_{j_2 l_2}(r'|\ \varepsilon_i \pm \omega)\ /\ (rr')^2 | , \right] \qquad \text{(I-4)}$$

when $r < r'$, r and r' are interchanged on the right side of eq. (I-4) when $r > r'$. The index i stands for the quantum numbers (n, l_1, j_1, S_1) of a bound state and f_i for the occupation factors. The summation is over all indices except I and over both + ω and - ω. For the case of - ω, the complex conjugates of all outgoing waves in eq. (I-4) are to be used. Angular momentum coupling coefficients are expressed in terms of Wigner 3j and 6j symbols.

REFERENCES

1. U. Fano and J.W. Cooper, Rev. Mod. **40**, 441 (1986).
2. M.J. Stott and E. Zaremba, Phys. Rev. A **21**, 12 (1980).
3. A. Zangwill and P. Soven, Phys. Rev. A **21**, 1561 (1980).
4. D. Liberman and A Zangwill, Comput. Phys. Commun. **32**, 75 (1984).
5. R. Haensel, G. Keitel, P. Schreiber and C. Kunz, Phys. Rev. **188**, 1375 (1969).
6. D.J. Kennedy and S.T. Manson, Phys. Rev. A **5**, 227 (1972).
7. K.H. Tan and C.E. Brion, J. Electron Spectros. **13**, 77 (1978).
8. J.A.R. Samson, Advan. Atom. Mol. Phys. **2**, 178 (1966).
9. F.L. Mohler and C. Boeckner J. Res. NBS **3**, 303 (1929).
10. G.V. Marr and D.M. Creek, Proc. R. Soc. A. **304**, 233 (1968).
11. U. Gupta, M. Blaha and J. Davis, J. Phys. B. **17**, 3617 (1984).

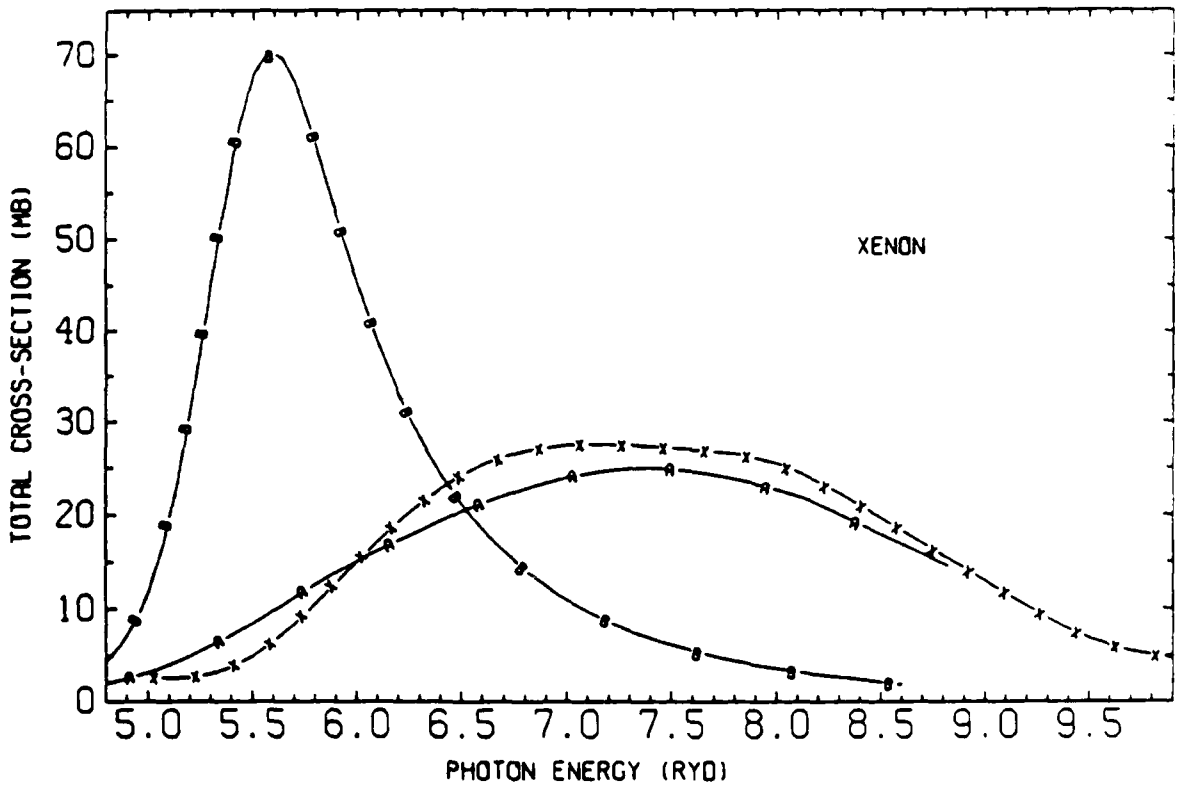

TOTAL PHOTOIONIZATION CROSS-SECTION OF NEUTRAL XENON NEAR 4D THRESHOLD. CURVE A: TIME DEPENDENT DENSITY FUNCTIONAL CALCULATION. CURVE B: INDEPENDENT PARTICLE MODEL: EXPERIMENTAL DATA FROM R. HANSEL ET. AL., PHYS. REV. 188, 1375 (1969)

Figure 1

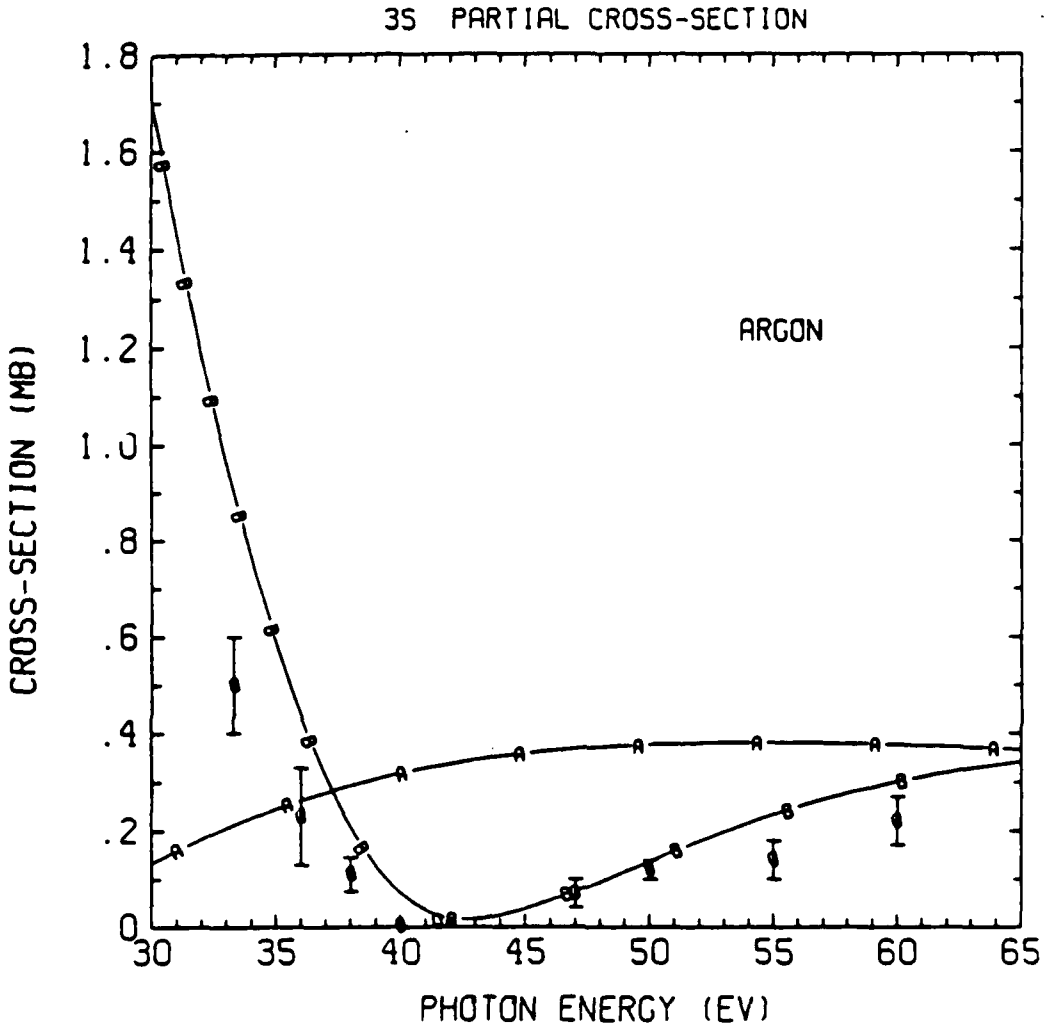

CURVE A: INDEPENDENT PARTICLE MODEL.

CURVE B: TIME-DEPENDENT DENSITY FUNCTIONAL CALCULATION.

DATA FROM K. TAN & C. BRION, J. ELECTRON SPECTROS. 13, 77(1978).

Figure 2

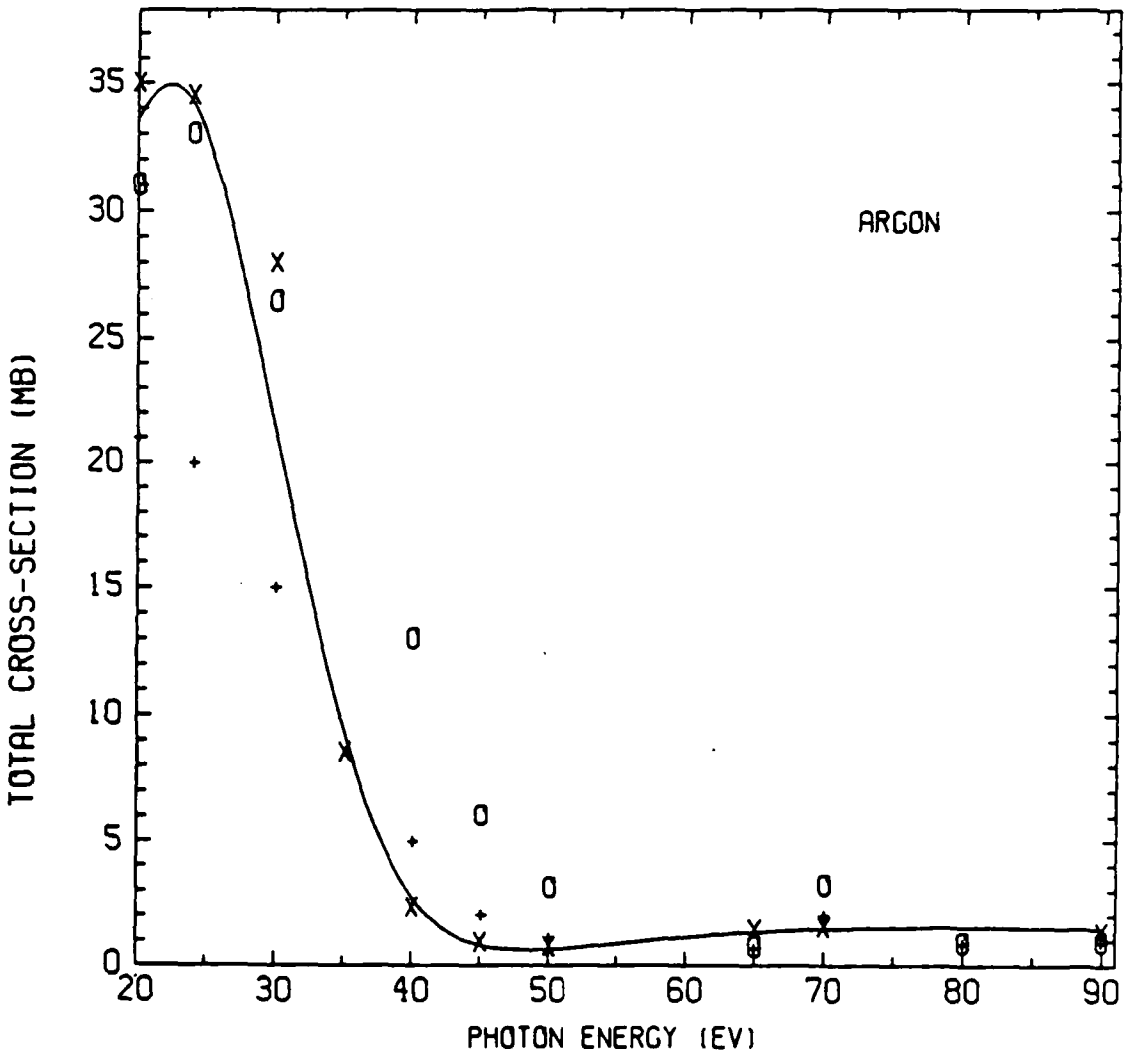

SOLID CURVE: TIME-DEPENDENT DENSITY FUNCTIONAL CALCULATION.
X: EXPERIMANTAL DATA FROM J.A.R.SAMSON, ADVAN. ATOM. MOL. PHYS. 2, 178(1966). +: HARTREE-FOCK (VELOCITY APPROX.) AND
O: HARTREE-FOCK (LENGTH APPROX.) BY KENNEDY & MANSON, PHYS. REV. A 5, 227(1972).

Figure 3

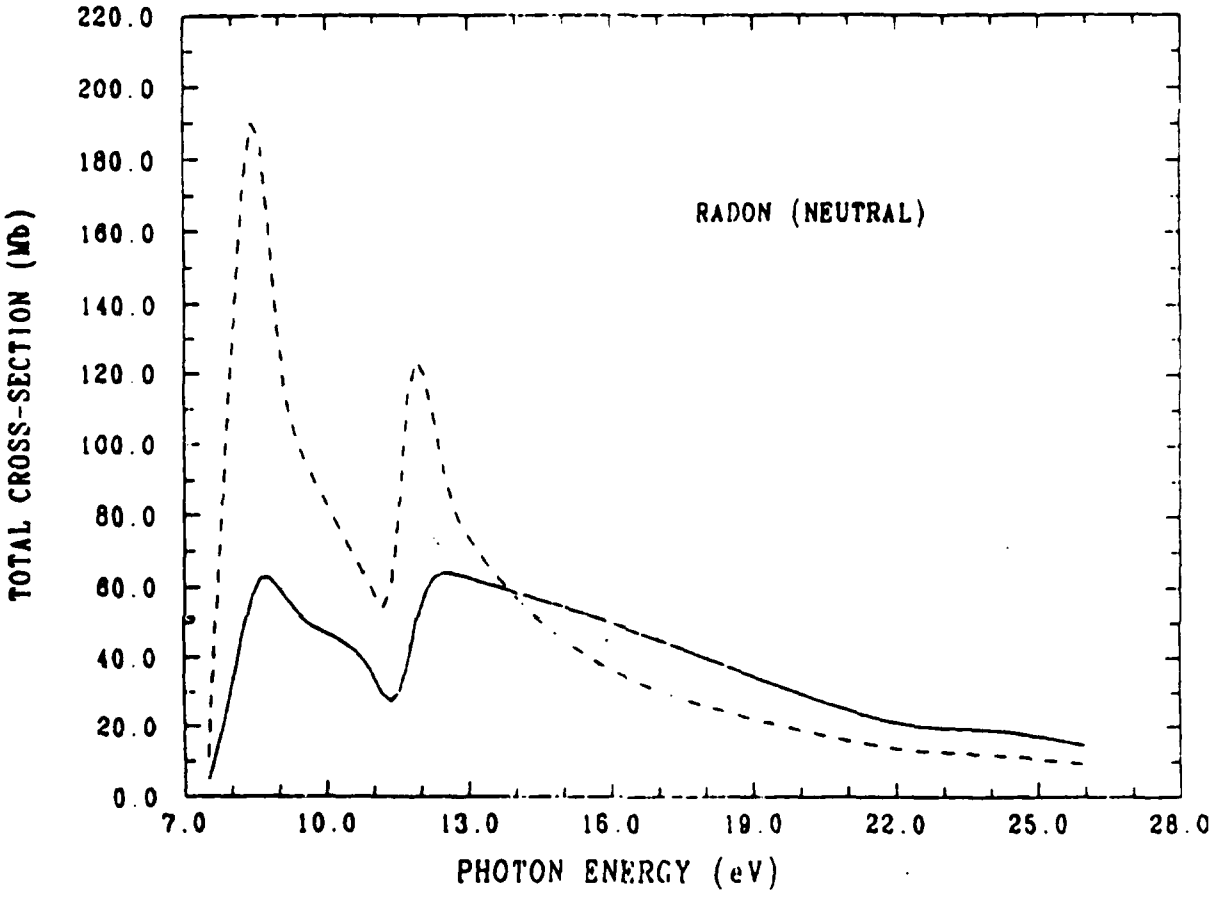

Solid Curve: Time-dependent density functional calculation
Dashed Curve: Independent particle model

Figure 4

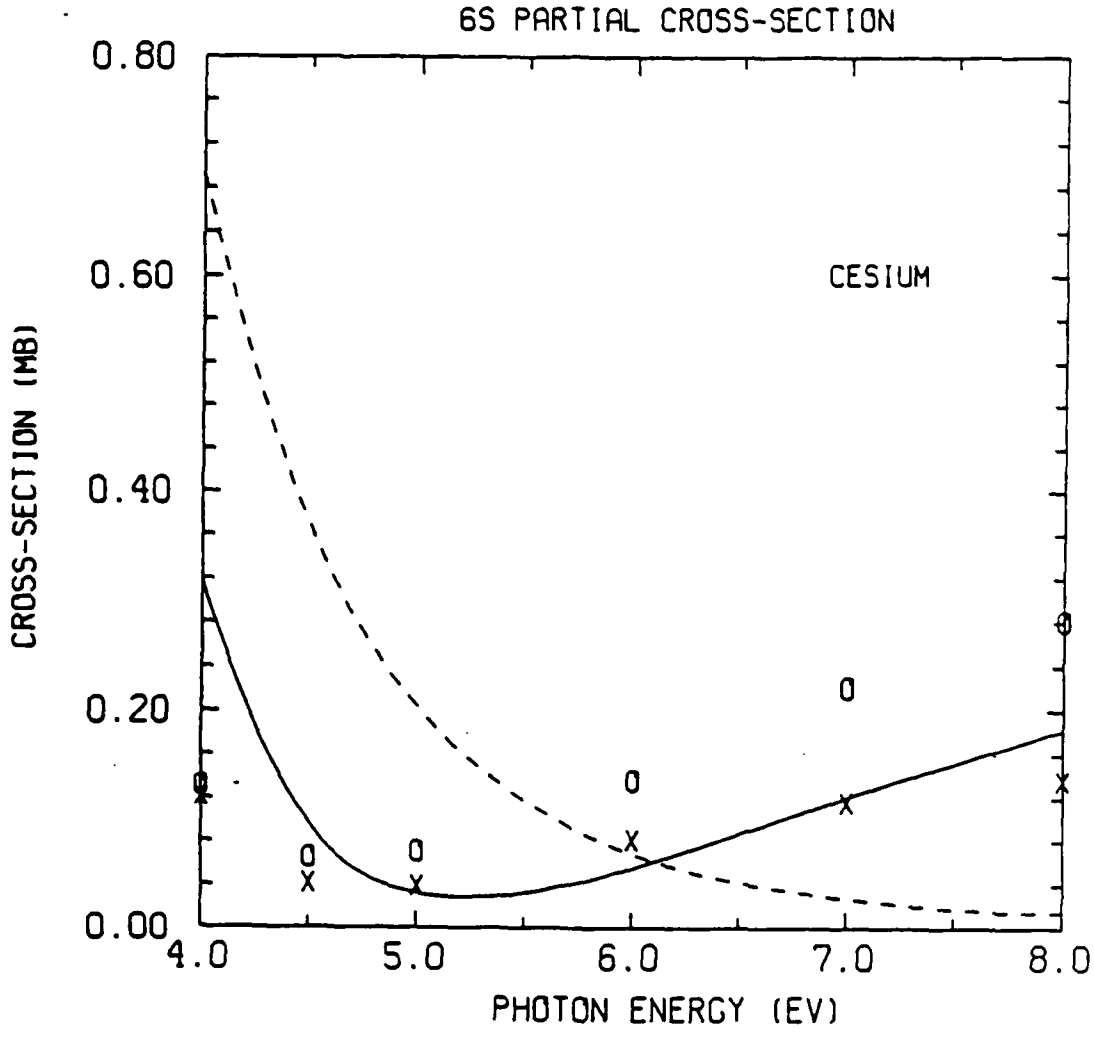

SOLID CURVE: TIME-DEPENDENT DENSITY FUNCTIONAL CALCULATION.
DASHED CURVE: INDEPENDENT PARTICLE MODEL.
X: EXPERIMENTAL DATA FROM MOHLER AND BOECKNER, J. RES. NBS 3, 303 (1929). O: EXPERIMENTAL DATA FROM MARR AND CREEK, PROC. R. SOC. A 304, 233 (1968).

Figure 5

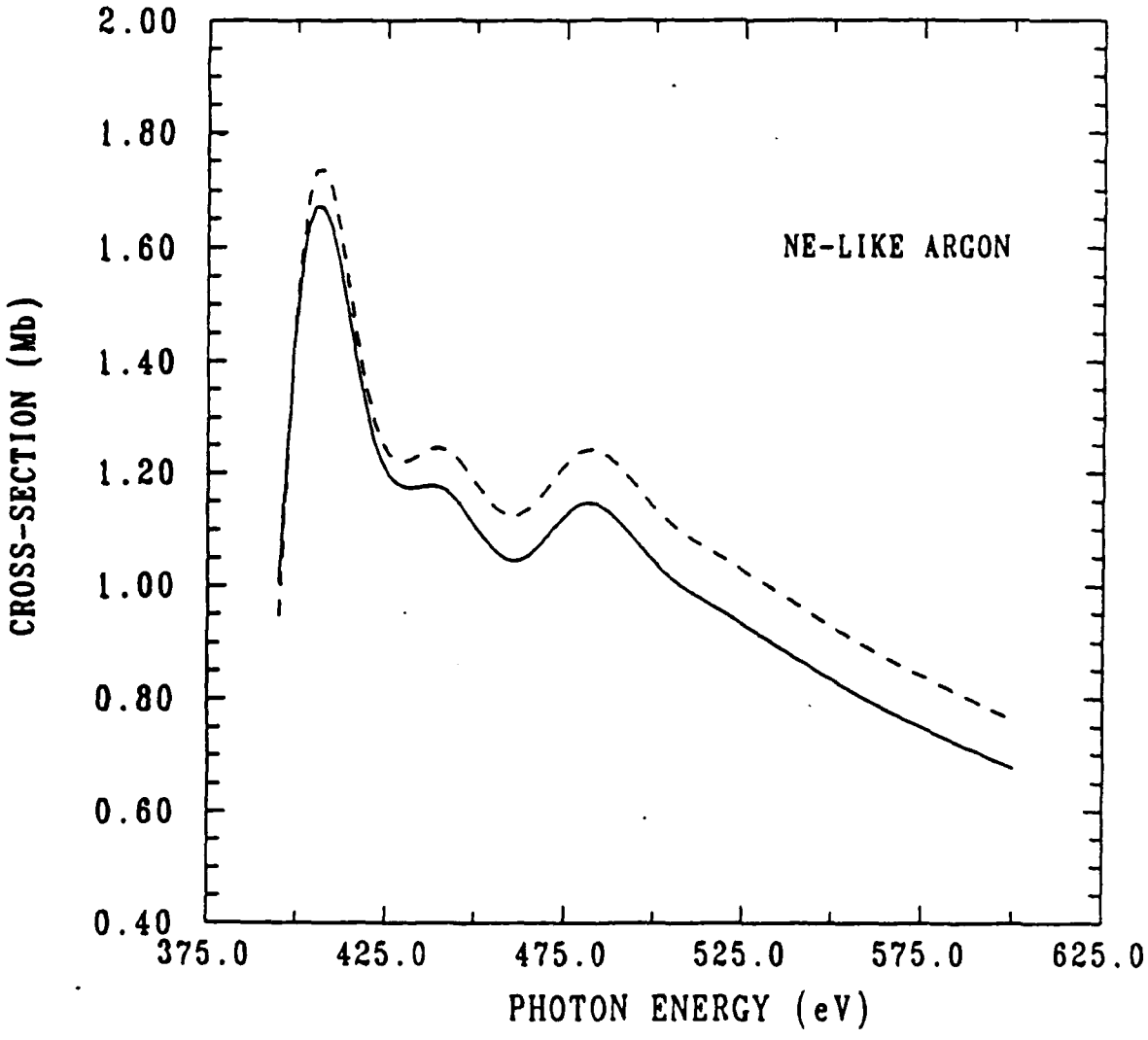

Solid Curve: Independent particle model.
Dashed Curve: Time-dependent density functional calculation.

Figure 6

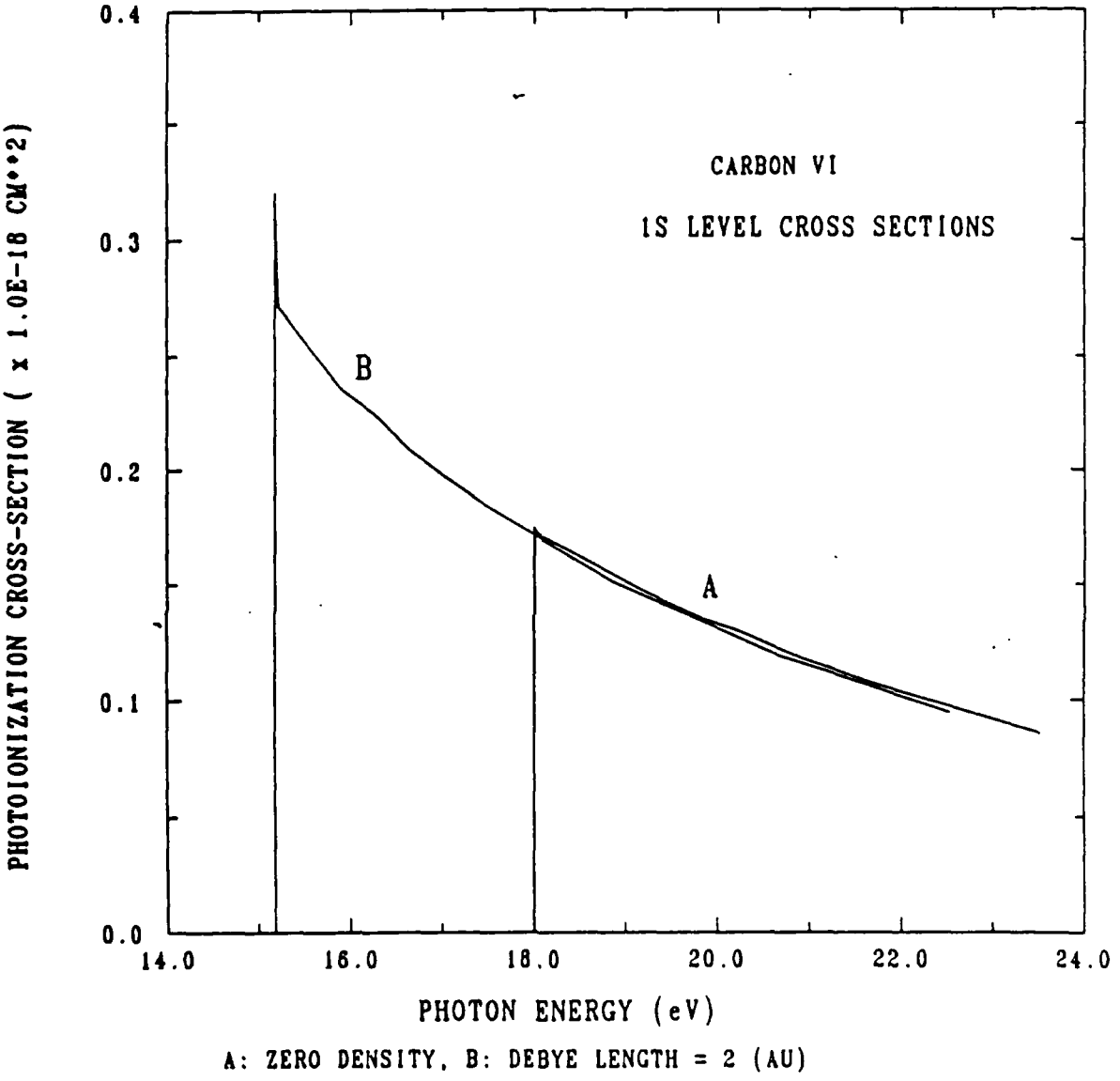
CARBON VI
1S LEVEL CROSS SECTIONS
B
A
PHOTOIONIZATION CROSS-SECTION (x 1.0E-18 CM**2)
0.4
0.3
0.2
0.1
0.0
14.0
16.0
18.0
20.0
22.0
24.0
PHOTON ENERGY (eV)
A: ZERO DENSITY, B: DEBYE LENGTH = 2 (AU)

Figure 7

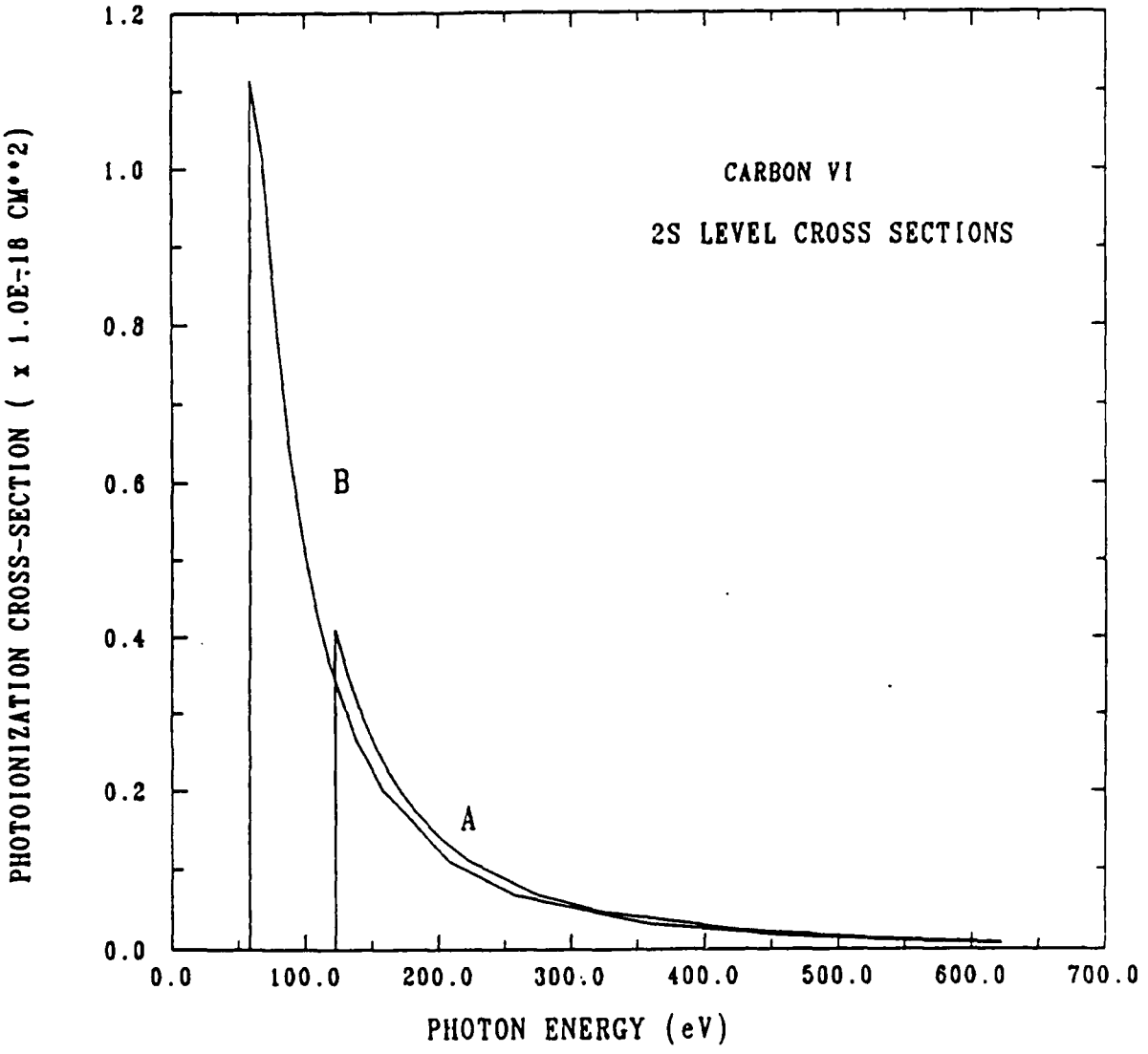

A: ZERO DENSITY, B: DEBYE LENGTH = 2 (AU)

Figure 8

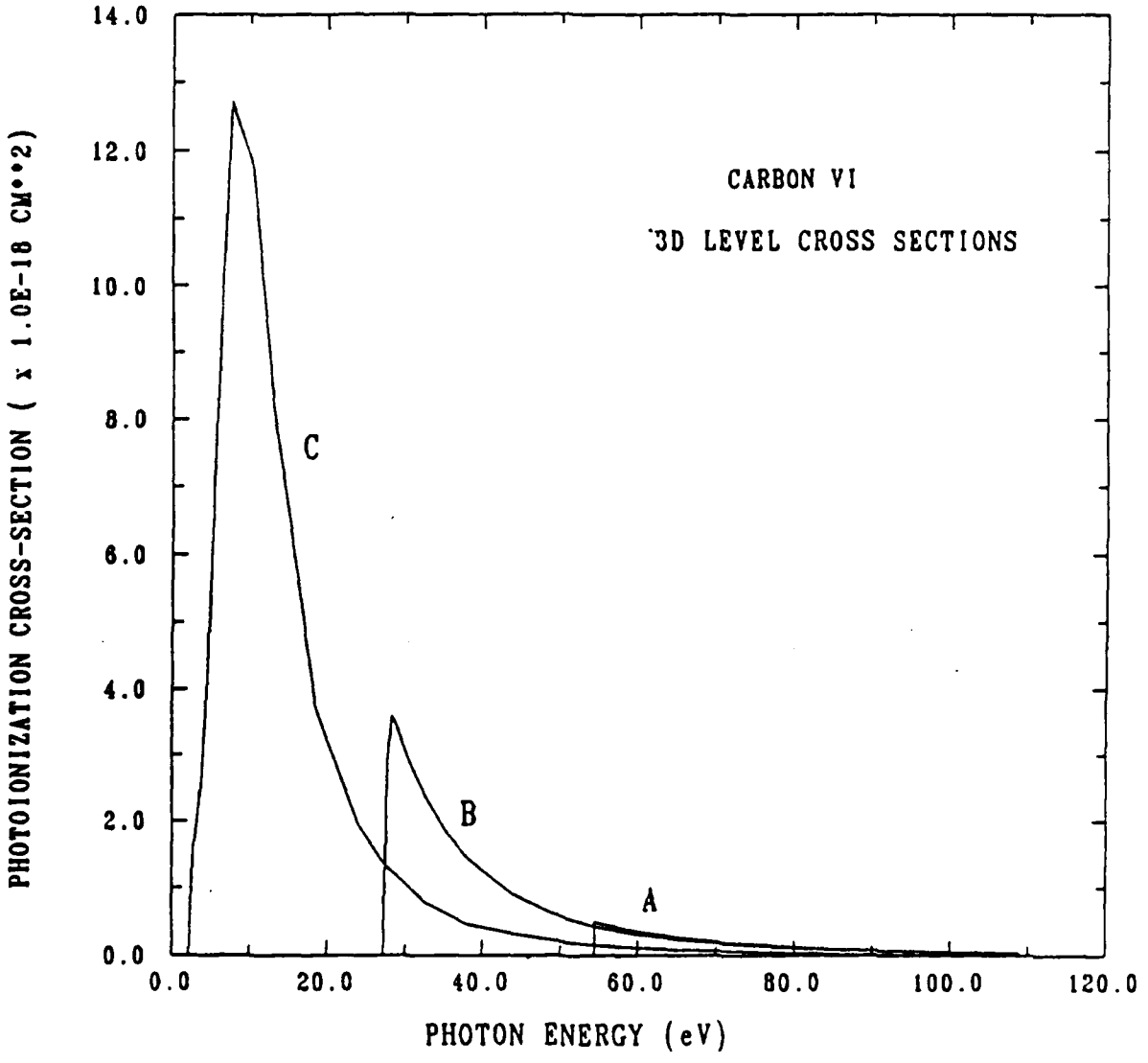

A: ZERO DENSITY, B: DEBYE LENGTH = 5 (AU)
C: DEBYE LENGTH = 2 (AU).

Figure 9

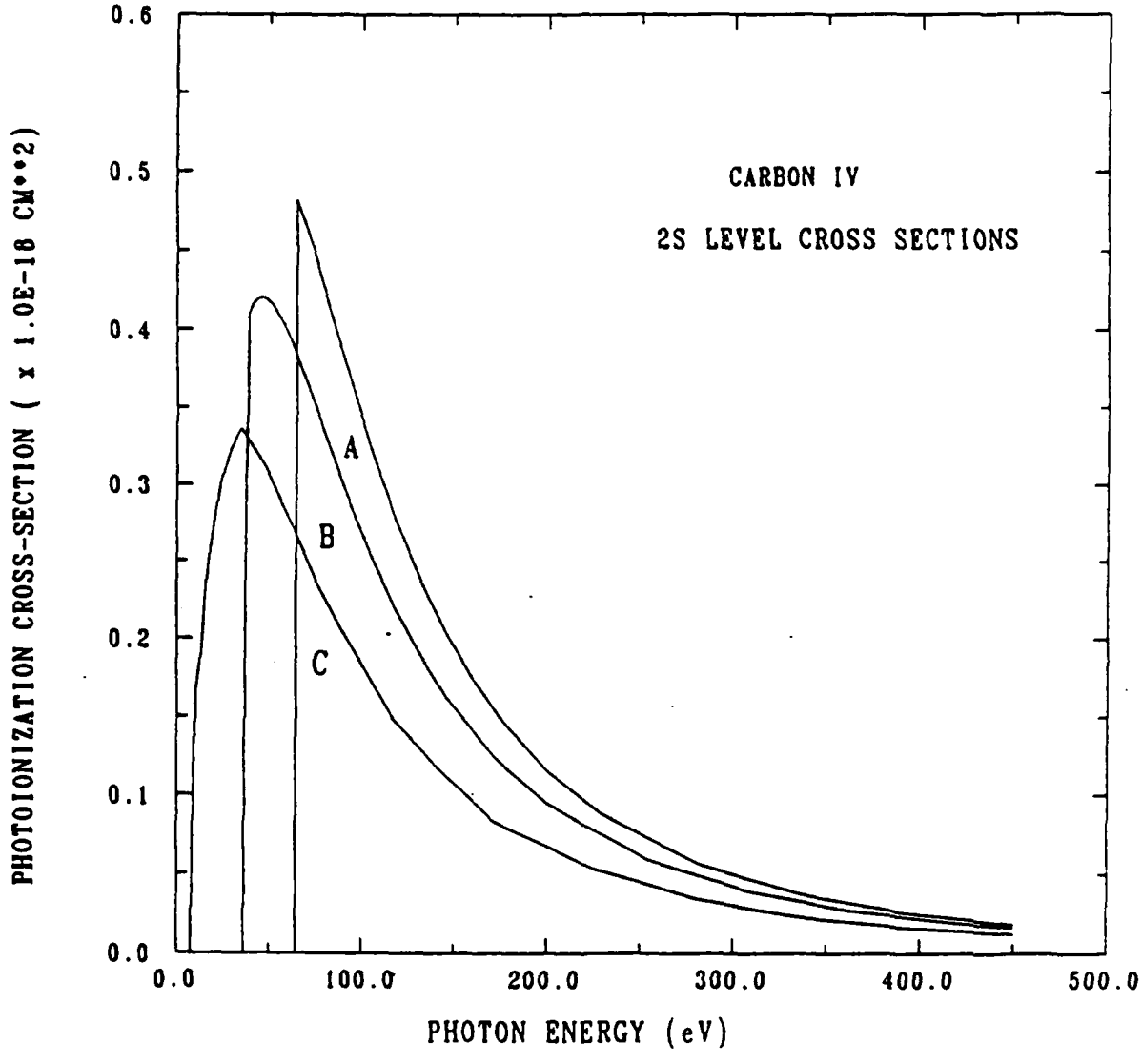

A: ZERO DENSITY, B: DEBYE LENGTH = 5 (AU)
C: DEBYE LENGTH = 2 (AU).

Figure 10

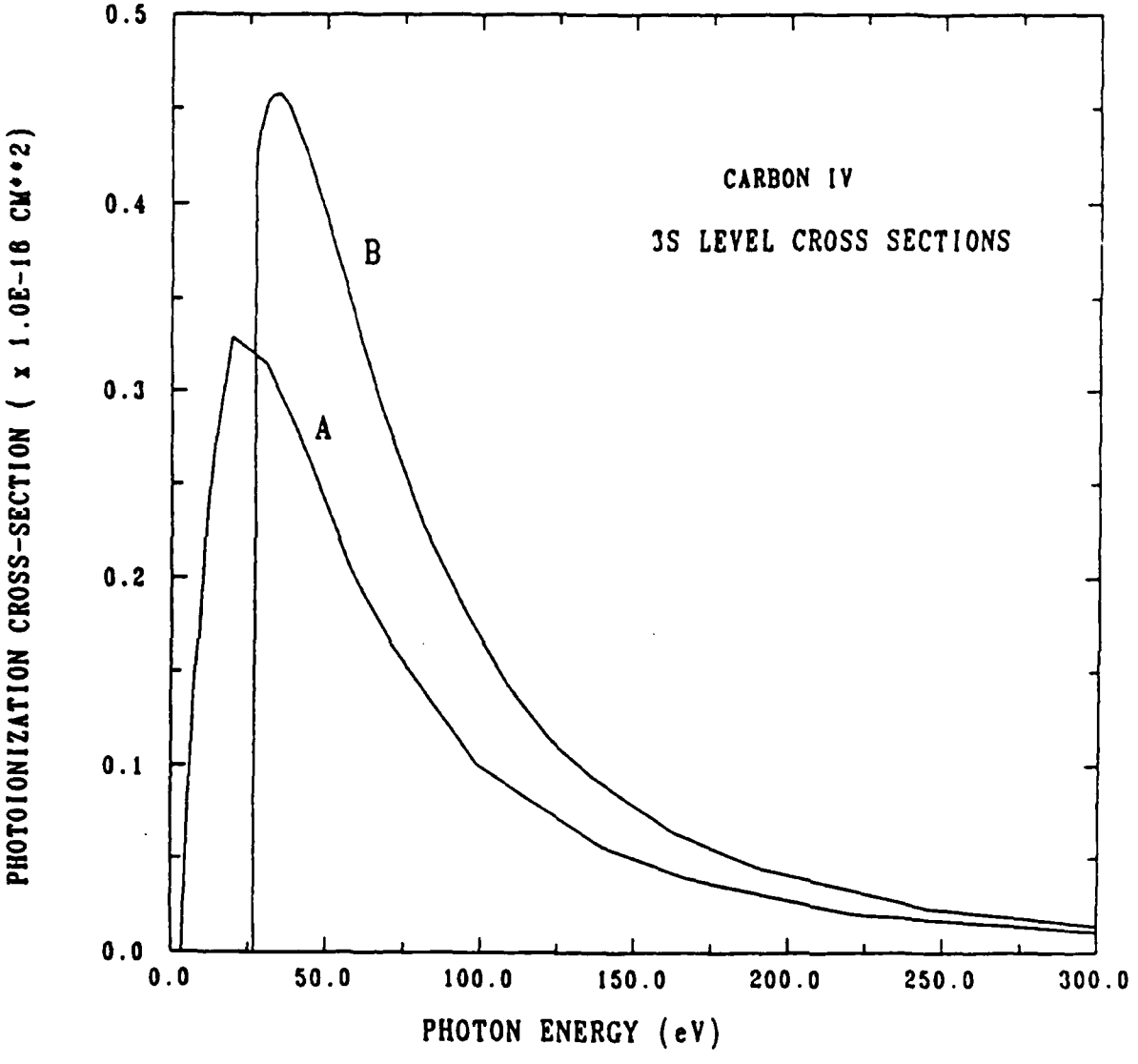

A: ZERO DENSITY, B: DEBYE LENGTH = 5 (AU)

Figure 11

DISTRIBUTION LIST

Larry Altgilbers
3805 Jamestown
Huntsville, AL 35810

Argonne National Lab
9700 S. Cass Avenue
Argonne, IL 60439
Attn: Y.-K. Kim
K.T. Lu, K105

Lloyd Armstrong
Department of Physics
Johns Hopkins University
Baltimore, MD 21318

P. Bakshi
Dept. of Physics and
Center for Energy Research
Boston College
Chestnut Hill, MA 02167

C. F. Barnett
Oak Ridge Natl. Lab
P. O. Box X
Bldg. 6003
Oak Ridge, TN 37830

Rogers Bengston
Dept. of Physics
U. of Texas
Austin, TX 78712

Klaus H. Berkner
Lawrence Berkeley Lab
Univ. of California
Berkeley, CA 94530

Nat Bhaskar
Columbia University
Columbia Radiation Lab
New York, NY 10027

Prof. L. C. Biedenharn
Duke University
Department of Physics
Durham, North Carolina 27706

Howard C. Bryant
Physics and Astronomy
Univ. of New Mexico
Albuquerque, NM 87131

J. T. Chan
Physics Department
Univ. of Arkansas
Fayetteville, AK 72701

Edward S. Chang
Department of Physics
Univ. of Massachusetts
Amherst, MA 01003

Shih-I Chu
Dept. of Chemistry
University of Kansas
Lawrence, KS 66045

David A. Clark
Univ. of New Mexico
P.O. Box 608
Albuquerque, NM 87544

E. D. Commins
Department of Physics
Univ. of California
Berkeley, CA 94720

William E. Cooke
Department of Physics
Univ. of S. California
University Park
Los Angeles, CA 90007

Stuart Crampton
Williams College
Williamstown, MA 01267

William A. Davis
Fusion Energy Division
Oak Ridge National Lab
Box Y, Building 9201-2
Oak Ridge, TN 37830

Hans G. Dehmelt
Department of Physics
Univ. of Washington
Seattle, WA 98195

Alan Desilva
University of Maryland
Physics Dept.
College Park, MD 20742

Richard D. Deslattes
National Science Foundation
Washington D.C. 20234

Norval Fortson
University of Washington
Seattle, WA 98105

Frank Franz
Dept. of Physics
Indiana University
Bloomington, IN 47405

Richard Freeman
Bell Laboratories
4D-321
Crawfords Corner Road
Homdel, NJ 07733

Robert S. Freund
Bell Laboratories
600 Mountain Avenue
Murray Hill, NJ 07974

G. Gerdin
214 Nucl. Eng. Lab.
1035 Goodwin
Urbana, IL 61801

K. I. Golden
Dept. of Electrical Engineering
Northeastern University
Boston, MA 02115

Harvey Gould
Bldg. 70, Room 257
Lawrence Berkeley Lab
Berkeley, CA 94720

Hans Griem
University of Maryland
Lab. for Plasma & Fusion Energy Studies
College Park, MD 20742

R. Gupta
University of Arkansas
Department of Physics
Fayetteville, AK 72701

Harvard University
60 Garden Street
Cambridge, MA 02138
W. H. Parkinson
Center for Astrophysics
Alex Dalgarno
Lyman Laboratory
Francis M. Pipkin

Roger A. Hegstrom
Dept. of Chemistry
Wake Forest University
Winston-Salem, NC 27109

Robert M. Hill
SRI International
333 Ravenswood Avenue
Menlo Park, CA 94025

Alan L. Hoffman
Mathematical Sciences Northwest
P. O. Box 1887
Bellevue, WA 98009

Harry C. Jacobson
Dir. of Special Programs
University of Tennessee
Knoxville, TN 37916

Duane H. Jaecks,
Physics Department
University of Nebraska
Lincoln, NE 68588

Thomas H. Jeys
Rice University
Space Phys. and Astronomy
6100 South Main
Houston, TX 77005

JILA/NBS
Campus Box 440
Univ. of Colorado
1510 Eisenhower Drive
Boulder, CO 80309
J. Cooper
Sidney Geltman
Nely Padial
Stephen J. Smith

Charles E. Johnson
Physics Department
N. Carolina State Univ.
Raleigh, NC 27607

W. R. Johnson
Physics Department
Univ. of Notre Dame
Notre Dame, IN 46556

B. R. Junker
ONR Code 323
800 North Quincy Street
Arlington, VA 22217

G. Kalman
Dept. of Physics and
Center for Energy Research
Boston College
Chestnut Hill, MA 02167

Kansas State University
Physics Department
Manhattan, KA 66506
Chander P. Bhalla
C. D. Lin

Univ. of Virginia
Physics Department
McCormick Road
Charlottesville, VA 22901
Hugh R. Kelly
Tom Gallagher

KMS Fusion, Inc.
P.O. Box 1567
3621 S. State Road
Ann Arbor, MI 48106
George Charatis
Jon T. Larsen
Paul Rockett
D. Tanner

Joseph J. Kubis
P.O. Box 1082
Ann Arbor, MI 48106

Lawrence Livermore National Laboratory
P.O. Box 808
Livermore, CA 94550
Attn: Hugh E. DeWitt
Richard Fortner, L-401
Abraham Goldberg
Forrest J. Rogers
Balazs F. Rozsnyai, L-71
James H. Scofield
Bruce W. Shore

Los Alamos Scientific Laboratory
P. O. Box 1663
Los Alamos, NM 87545
Attn: Fred Begay (1 each)
John H. Brownell, M.S. 220
Lee A. Collins
C. W. Cranfill, M.S. 538
R. Godwin, M.S. 420
Alan Hauer, M.S. 554
Walter F. Huebner, MS-212
Larry Jones, MS-455
Joseph B. Mann
A. L. Merts
T. F. Stratton

Massachusettes Institute of Technology
Cambridge, MA 02139
Shaoul Ezekiel
Rm. 26-255
Michael Feld
Room 6-009
Daniel Kleppner
Room 26-231

Harold J. Metcalf
Physics Department
State University of NY
Stony Brook, NY 11794

Fred W. Meyer
Oak Ridge National Lab
P.O. Box X
Bldg. 6003
Oak Ridge, TN 37830

Masataka Mizushima
Physics Department
Univ. of Colorado
Boulder, CO 80309

National Bureau of Standards
Washington, D.C. 20234
Attn: Larry Roszman (1 Each)
Raju U. Datla, Bldg. 221
Joseph Reader
Wofgang Wiese,
Bldg. 221, Rm. A267

Univ. of Illinois
Dept. of Physics
Chicago Campus
Urbana, IL 61801
Attn: M. H. Nayfeth
C. Rhodes

Randolph S. Peterson
Box U-46
Dept. of Physics
Univ. of Conn.
Storrs, CT 06268

Robert Peterson
Nuclear Engineering Dept.
University of Wisconsin
1500 Johnson Drive
Madison, Wisconsin 53706

Physics International Inc.
2700 Merced Street
San Leandro, CA 94577
Richard L. Schneider
M. Krishnan

H. Pilloff
ONR Code 323
800 N. Quincy St.
Arlington, VA 22217

Michael S. Pindzola
Oak Ridge National Lab
Phys. Div., Bldg. 6003
Oak Ridge, TN 37830

Princeton University
Plasma Physics Laboratory
Forrestal Campus
Princeton, NJ 08540
Manfred L. Bitter
Kenneth W. Hill

A. K. Rajagopal
Dept. of Physics and Astronomy
Louisiana State University
Baton Rouge, LA 70803

A. R. P. Rau
Physics & Astronomy
Louisiana State Univ.
Baton Rouge, LA 70803

M. Eugene Rudd
University of Nebraska
Behlen Lab of Physics
Lincoln, NB 68588

D. H. Sampson
Dept. of Astronomy
525 Davey Laboratory
Pennsylvania State Univ.
University Park, PA 16802

Wolfgang Sandner
SRI International
332 Ravenswood Avenue
Menlo Park, CA 94025

Ivan A. Sellin
Oak Ridge National Lab
P.O. Box X
Oak Ridge, TN 37830

Robin Shakeshaft
Department of Physics
Texas A & M University
College Station, TX 77843

R. Shepherd
Dept. of Nuclear Eng.
114 N.A.M.E.
Ann Arbor, MI 48106

Haward A. Shugart
Department of Physics
Univ. of California
Berkeley, CA 94720

Rolf Sinclair
Physics Division
Natl. Sci. Foundation
Washington, D.C. 20550

Ken Smith
Rice University
Space Phys. and Astronomy
6100 South Main
Houston, TX 77005

Winthrop W. Smith
Department of Physics
Univ. of Connecticut
Storrs, CT 06268

Larry Spruch
New York University
Physics Department
4 Washington Place
New York, NY 10003

Stanford University
Stanford, CA 94305
ATTN: Nils Carlson (1 each)
S. E. Harris
Edward L. Ginzton Lab
W. E. Meyerhof
Arthur L. Schawlow

Ronald F. Stebbings
Dept. of Space and Astron.
Rice University
Houston, TX 77001

Rudolph M. Sternheimer
Dept. of Physics
Brookhaven National Lab.
Upton, NY 11973

Strategic Defense Initiative Organization
Pentagon
Washington, D. C. 20301-7100
Attn: Dwight Duston
James Ionson
Len Caveny

University of Florida
Department of Physics
Gainesville, FL 32611
Attn: C.F. Hooper, Jr. (1 each)

University of Michigan
Physics Department
500 E. University
Ann Arbor, MI 48109
Terry Kamish
Dept. of Nuclear Eng.
W. L. Williams
3044 Randall Lab
Jens C. Zorn

University of Rochester
Lab. for Laser Energetics
250 E. River Road
Rochester, NY 14623
Reuben Epstein
Stanley Skupsky

University of Pittsburgh
Pittsburgh, PA 15260
ATTN: J. E. Bayfield (1 each)
Physics Department
100 Allen Hall
Dr. Richard H. Pratt

L. Vahala
Dept. of Elec. Eng.
Old Dominion University
Norfolk, VA

Carol Venanzi
Rutgers University
P. O. Box 939
Piscataway, NJ 08854

Leposava Vuskovic
Jet Propulsion Lab
4800 Oak Grove Drive
Pasadena, CA 91103

Fred L. Walls
Natl. Bur. of Standards
325 Broadway
Boulder, CO 80303

Shinichi Watanabe
Dept. of Physics
University of Chicago
1100 East 58th Street
Chicago, IL 60637

William Westerveld
Department of Physics
N. Carolina State Univ.
Raleigh, NC 27650

William Wing
Phys. and Optical Sciences
University of Arizona
Tucson, AZ 85721

Peter Winkler
Physics Department
University of Nevada
Reno, Nevada 89557

David M. Woodall
Dept. of Nuclear Engineering
University of New Mexico
Albuquerque, NM 87131

Robert Yaris
Chemistry Department
Washington University
St. Louis, MO 63130

Naval Research Laboratory
Washington D. C. 20375
Code 4700 26 Copies
Code 4720 50 Copies
Dr. Philip G. Burkhalter, 6681
Dr. Raymond C. Elton, Code 4730
Dr. Ed McLean, Code 4730
Dr. Tung Nyong Lee, Code 4730

Code 2627 22

Code 1220 1

Director of Research
U.S. Naval Academy
Annapolis, MD 21402

Pierre Agostini
C.E.A.
CEN SACLAY
B.P. 2 Gif-sur-Yvette
FRANCE

Ignacio Alvarez
Instituto de Fisica
U.N.A.M.
Apdo. Pstal 20-364
MEXICO

Dr. Alain Angelie
Commissarait a l'Energie Atomique
Villeneuve St. Georges
FRANCE

Alain Aspect
Universite Paris Sud
B.P. 43
91406 Orsay Cedex
FRANCE

P.E.G. Baird
Clarendon Laboratory
University of Oxford
Parks Road
Oxford, ENGLAND

Gunter G. Baum
Univ. Bielefeld
Fakultat fur Physik
48 Bielefeld
WEST GERMANY

Uwe Becker
Tech. Univ. Berlin
Rondellstr. 5, D-1000
Berlin 37
WEST GERMANY

Biblioteque
21, Av. des Bains
CH-1007 Lausanne
SWITZERLAND

Emile Biemont
Inst. D'Astrophysique
Universite de Liege
B-4200 Cointe-Ougree
BELGIUM

J. L. Bobin
C. Etudes Limeil BP 27
94190 Villeneuve St. Georges
FRANCE

Norbert Bose
Univ. of Toronto
60 St. George Street
Toronto, M5S 1A7
CANADA

C. Bouchiat
Ecole Normale Sup.
24 Rue Lhomond 24
75231 Paris Cedex 05
FRANCE

Fritz Buchinger
Mainz University
CERN
CERN Div. EP
Geneve, SWITZERLAND

D. D. Burgess
The Blackett Laboratory
Imperial College of Science & Technology
London SW7 2BZ,
ENGLAND

Carmen Dra. Cisneros
Instituto de Fisica
U.N.A.M.
Apdo. Postal 20-364
MEXICO

Charles W. Clark
SRC Daresbury Lab.
Daresbury, Warrington
ENGLAND WA4 4AD

N. Czsjkowski
University of Windsor
Windsor, Ontario
CANADA N9B 3P4

C. Deutsch
Laboratoire de Physique des Plasmas
Universite Paris XI
91405 Orsay
FRANCE

Andre Dietrich
Tech. Univ. Berlin
D 1 Berlin 37
Rondellstrasse 5
WEST GERMANY

Gordon Drake
Department of Physics
University of Windsor
Windsor, Ontario
CANADA N9B 3P4

Francoise Fabre
C.E.A.
CEN SACLAY
B.P.2 Gif-sur-Yvette
FRANCE

Edmond Genenx
Universitat Bern
Sidlerstrasse
3012 Berne
SWITZERLAND

Elisabeth Giacobino
Universite Paris VI
4 Place Jussieu
75230 Paris Cedex 05
FRANCE

Samuel A. Goldman
University of Windsor
Windsor, Ontario
CANADA N9B 3P4

Dr. Francois Grimaldi
Centre D'Etudes de Limeil
Villeneuve, St. Georges
FRANCE

G. Friedrich Hanne
Physikal Institut
Correnssstrasse
4400 Muenster
WEST GERMANY

R. A. Holt
Dept. of Physics
Univ. of West. Ontario
London, Ontario
CANADA, N6A 3K7

J. W. Humberston
Univ. College London
Gower Street
London WC1E 6BT
ENGLAND

F. E. Irons
Hughes Technology Pty. Ltd.
P. O. Box 1155
Canberra
A.C.T. 2601
AUSTRALIA

P. Jaegle
Laboratoire de Spectroscopie
Atomique et Ionique
University Paris-Sud
Orsay, FRANCE

Dr. Takako Kato
Institute of Plasma Physics
Nagoya University, JAPAN

H. Klein
Clarendon Laboratory
Parks Road
Oxford
ENGLAND

Hans Kleinpoppen
Inst. of Atomic Phys.
University of Stirling
Stirling, FK94LA
ENGLAND

Aaron D. Krumbein
Soreq Nuclear Research Center
Yavne, ISRAEL 70600

Hans-Joach I. Kunze
Inst. Experimentalphysik V
Ruhr Universitat
Postfach 2148
4630 Bochum
WEST GERMANY

Dr. Michele Lamoureux
Laboratoire de Spectroscopie
Atomique et Ionique
Universite Paris-Sud
Orsay, FRANCE

W. N. Lennard
Atom. Ener. of Canada Ltd.
C.R.N.L.
Chaulk River, Ontario
CANADA KOJ 1JO

Librarian
Max-Planck-Institut fur Plasmaphysik
8046 Garching bei Munchen
WEST GERMANY

Library
Institut fur Plasmaforschung
Universitat Stuttgart
Pfaffenwaldring 31
700 Stuttgart 80
WEST GERMANY

H. O. Lutz
Univ. Bielefeld
Fakultat fur Physik
D-4800 Bielefeld 1
WEST GERMANY

Dr. M Stuart McRobert
Blackett Laboratory
Imperial College
ENGLAND

Reinhard Morgenstern
University Utrecht
Princetonplein 5
NL 3508 TA Utrecht
NETHERLANDS

Hajime Narumi
Dept. of Physics
Hiroshima University
Hiroshima 730
JAPAN

A. Ng
Dept. of Physics
U.B.C. Vancouver
B.C., CANADA V6T 1W5

Derek Paul
Physics Department
University of Toronto
Toronto M5S 1A7 CANADA

Dr. F. Perrot
Centre d'Etudes de Limeil
Villeneuve St. Georges
FRANCE

F. H. Read
Physics Department
Univ. of Manchester
Manchester M13 9P1
ENGLAND

Arne Rosen
Department of Physics
Chalmers Univ. of Tech.
S-41296 Goteborg
SWEDEN

S. David Rosner
Department of Physics
Univ. of Western Ontario
London, Ontario
N6A 3K7 CANADA

David Salzmann
Soreq Nuclear Research Center
Yavne 70600
ISRAEL

Joshua D. Silver
Univ. of Oxford
Parks Road
Oxford OX1 3PU
ENGLAND

A. C. H. Smith
Dept. of Phys. and Astro.
Univ. College London
London WC1E 6BT
ENGLAND

N. Stolterfoht
Hahn-Mfitner-Institut
D-1 Berlin 39
100 Glienickerstr.
WEST GERMANY

J. D. Talman
Department of Chemistry
Univ. of West. Ontario
London, Ontario
N6A 3K7 CANADA

Hiroshi Tanaka
Sophia University
Faculty of Sci. and Tech.
Chiyoda-Ku, Koiocho 7
Tokyo, JAPAN 102

F. Trager
Physikalisches Institut
Der Univ. Heidelberg
D-690 Heidelberg 1
WEST GERMANY

Ervin Weinberger
University of Toronto
255 Huron Street
Toronto, Ontario
CANADA M5S 1A7

Tatsuhiko Yamanaka
Osaka University
Osaka, JAPAN

Dieter Zimmermann
Inst. fur Strahlungs-Un
Kerenphysik
Technische Univ. of Berlin
D-1002 Berlin
WEST GERMANY

Zev Zinamon
The Weizmann Institute of Science
Rehovot, ISRAEL

END

12-87

DTIC